

CrystEngComm

Accepted Manuscript



This is an *Accepted Manuscript*, which has been through the RSC Publishing peer review process and has been accepted for publication.

Accepted Manuscripts are published online shortly after acceptance, which is prior to technical editing, formatting and proof reading. This free service from RSC Publishing allows authors to make their results available to the community, in citable form, before publication of the edited article. This *Accepted Manuscript* will be replaced by the edited and formatted *Advance Article* as soon as this is available.

To cite this manuscript please use its permanent Digital Object Identifier (DOI®), which is identical for all formats of publication.

More information about *Accepted Manuscripts* can be found in the [Information for Authors](#).

Please note that technical editing may introduce minor changes to the text and/or graphics contained in the manuscript submitted by the author(s) which may alter content, and that the standard [Terms & Conditions](#) and the [ethical guidelines](#) that apply to the journal are still applicable. In no event shall the RSC be held responsible for any errors or omissions in these *Accepted Manuscript* manuscripts or any consequences arising from the use of any information contained in them.

ARTICLE

Exploring coral biomineralization in gelling environments by means of the counter diffusion system

Cite this: DOI: 10.1039/x0xx00000x

Received 00th January 2012,
Accepted 00th January 2012

DOI: 10.1039/x0xx00000x

www.rsc.org/

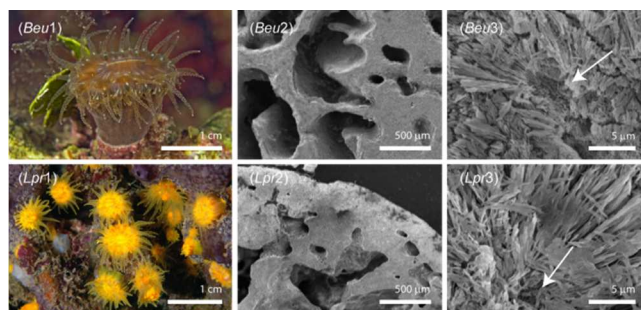
M. Sancho-Tomás^a, S. Fermani^b, S. Goffredo^c, Z. Dubinsky^d, J.M. García-Ruiz^a, J. Gómez-Morales^{*a} and G. Falini^{ab}

The crystallization of skeletal aragonite by corals takes place in sites whose physical characteristics resemble those of a highly viscous sol or a gel. In these sites biomolecules are secreted by calicoblast cells of the coral and some of them become entrapped in the skeleton. To explore the biomineralization process a series of calcium carbonate crystallization experiments were carried out in a counter-diffusion system (CDS) containing an agarose viscous sol with two dissolved intra-skeletal soluble organic matrices (SOM) that were extracted from *Balanophyllia europaea*, a zooxanthellate coral, and *Leptopsammia pruvoti*, an azooxanthellate species. The influence of the viscosity of the media and the presence of Mg²⁺ were investigated in two additional sets of experiments, one using an agarose gel of variable viscosity, and another allowing Mg²⁺ to diffuse from the cationic reservoir. The main findings are the following: (i) the species-specific molecular composition of the two SOMs has a different impact on the crystallization parameters and morphology of calcium carbonate; (ii) the viscosity of the gelling media, and thus its porosity, is important in regulating the SOM action; (iii) Mg²⁺ is important in defining specific, and sharp, limits of supersaturation under which crystallization occurs; (iv) the polymorph distribution is determined by SOM concentration. Thus, through the use of the CDS, it was possible to first study *in vitro* the biomineralization of a zooxanthellate and azooxanthellate corals.

1 Introduction

2 Scleractinia corals represent the biggest source of biogenic calcium carbonate^{1, 2} on Earth and are among the fastest marine
3 mineralizing organisms.³ Despite their great contribution to oceanic biomineralization,⁴ many aspects of their mechanism of
4 mineralization are still a source of discussion and controversy. It has long been recognized that coral skeletons comprise both
5 inorganic (aragonite) and organic components,^{5, 6} but the level of biological control over calcification is still an open issue. The
6 scleractinian skeleton (Fig. 1) is composed of groups of needle-like aragonite crystals that radiate out from the *center of*
7 *calcification*,⁷ rich in calcium and sulphur.^{8, 9} This structural organization is controlled by specific macromolecules and is only
8 slightly affected by external environmental parameters.
9 Coral mineralizes at the interface between the polyp's calicodermic tissue and the skeleton. This region is extremely rich in
10 glycoproteins and glycosaminoglycans able to bond water molecules, thus the coral mineralization site was suggested to have the
11 features of a highly viscous sol.¹⁰ An amorphous organic membrane was observed between the calicodermis and the skeleton and
12 it was postulated that the site of mineralization is a colloidal gel matrix.¹¹
13 Recent researches suggested that there is a pathway involving direct seawater transport to the calcifying media in coral, which
14 links the site of calcification to the surrounding ocean.¹² Others similar *in vivo* experiments showed that seawater acidification
15 leads to a gradual relative decrease of pH of the medium in the calcification site, leading to an increasing pH difference between
16 the calcification site and seawater.¹³ The direct sea water transport to the calcification site implies that the precipitation of
17 aragonite could be due to the high content of Mg²⁺ in seawater, with respect to calcium ions¹⁴ (Mg/Ca molar ratio equal to 5).
18 However, the control of the local saturation state at the nucleation site requires the involvement of biological macromolecules,
19 which are secreted by the calicoblast cells. The role of these macromolecules is also the control of the structural and textural
20 organization of the mineral regions of the skeleton. Moreover, their activity could be regulated by the presence of Mg²⁺.²⁻⁴
21 Goffredo *et al.*¹⁵ showed that the intra-skeletal organic matrix from the Mediterranean solitary zooxanthellated coral *Balanophyllia*

22 *europaea* favours the precipitation of aragonite and that this occurs through a transient phase of amorphous calcium carbonate
 23 stabilized by lipids. Furthermore, they showed that the organic matrix molecules also controlled the morphology of the precipitated
 24 calcium carbonate crystals. The influence of coral intra-skeletal organic matrix in the precipitation of calcium carbonate (CaCO₃)
 25 has been also demonstrated for the tropical species *Acropora digitifera*, *Lophelia pertusa* and *Montipora calculata*.¹⁶ This study
 26 highlighted the importance of the low molecular weight macromolecules in the control of calcium carbonate polymorphism. An
 27 important recent research has shown that four highly acidic proteins, derived from expression of genes obtained from the common
 28 stony coral, *Stylophora pistillata*, can spontaneously catalyse the precipitation of aragonite *in vitro* from seawater.¹⁷ However,
 29 despite these advances, the chemical and physical processes that take place at the nucleation site are still only partly understood.

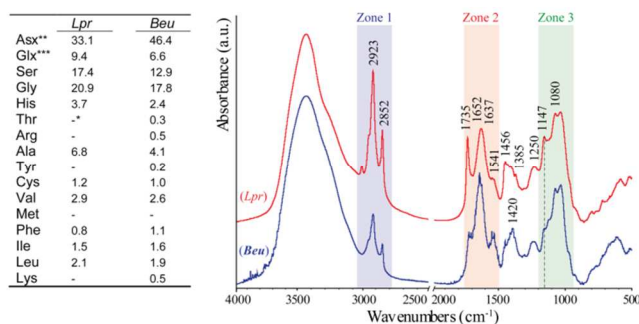


30 Figure 1. Underwater *in situ* camera pictures of *B. europaea* (Beu1) and *L. pruvoti* (Lpr1). SEM cross section images of the skeleton of *B. europaea* (Beu2, 3) and *L.*
 31 *pruvoti* (Lpr2, 3) are also shown. In them the different macroscale organization of the septa and microscale organization of the aragonitic fibers and of the centers of
 32 calcification is evident. The arrows indicate centers of calcification surrounded by aragonite fibers.
 33

34 In the present study, the crystallization of calcium carbonate was carried out in a counter diffusion system (CDS)^{18, 19} using a
 35 highly viscous agarose sol or an agarose gel²⁰ in which the intra-crystalline soluble organic matrix (SOM) extracted from the
 36 solitary Mediterranean corals (Fig. 1) *B. europaea* (BeuSOM), zooxanthellate, or *L. pruvoti* (LprSOM), azooxanthellate, was
 37 added. These two species differ for the presence of symbiotic photosynthetic algae (zooxanthellae), which provide the main
 38 energetic support to corals that host them,^{21, 22} and are thought to facilitate calcification by raising the pH in their proximity. The
 39 CDS method^{23, 24} was proved to be a valid tool in the study of biomineralization processes,^{25, 26} allowing to discriminate between
 40 inhibition/promotion of an additive on the nucleation/growth processes. The aim of the present study is to understand the influence
 41 of SOM in the precipitation of calcium carbonate in environments with different viscosities and to test the role of diffusing Mg²⁺.

42 Results

43 **Overview on SOMs composition.** The SOMs were characterized by their amino acid composition and FTIR spectroscopy (Fig.
 44 2). The amino acid composition was in agreement with that observed in many intra-skeletal acidic macromolecules. It was
 45 characterized by a high content of aspartic (and asparagine) and glutamic (and glutamine) residues.

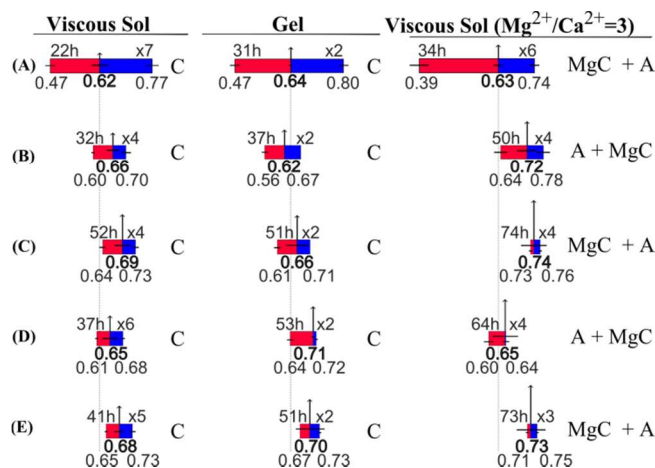


46 Figure 2. Left, amino acid composition of the SOMs from *B. europaea* and *L. pruvoti*. The amino acid content is reported as mol percentage. Some amino acids were
 47 not detected and some chromatographic signal could not be assigned. For this reason the sum of the amino acid percentages is lower than 100. Right, FTIR spectra
 48 from the SOMs from *B. europaea* (Beu) and *L. pruvoti* (Lpr). In the figure three zones (1-3) are highlighted, they correspond to regions where the main absorption
 49 bands due to lipids, proteins and polysaccharides, respectively, are located. The dotted line indicates an absorption band typical of sulphate groups.
 50

51 The carboxylate bearing residues (*Asx* and *Glx*) represented the 52.0 and the 42.5 mol % of residues in *BeuSOM* and *LprSOM*,
 52 respectively; in the latter a higher content of *Ser* and *Gly* (17.4 and 20.9) was present with respect to the former (12.9 and 17.8).
 53 The FTIR spectra showed that *BeuSOM* had, with respect to *LprSOM*, a lower absorption in the bands in zone 1 and a different
 54 structure of the bands in zone 3, which were due to methyl and methylene functional groups and glycosidic ether groups,

55 respectively. The *Lpr*SOM also showed a stronger absorption in the bands at 1147 cm^{-1} , which could be associated to the sulphate
56 group.²⁷

57 **Calcium carbonate precipitation in the highly viscous sol by CDS.** A reference experiment of calcium carbonate crystallization
58 was carried out by diffusing, in the agarose highly viscous sol, a 0.5 M calcium chloride solution from the cationic reservoir and a
59 0.5 M sodium hydrogen carbonate solution from the anionic one. The measured parameters in the U-tube set-up, as defined in the
60 experimental section, are the following: t_w (waiting time), x_o (starting point of precipitation) and Δ (crystal growing space). The
61 first precipitate appeared after a t_w of 22 ± 8 hr at x_o position equal to 0.62 ± 0.05 . The precipitation evolved symmetrically with
62 respect to x_o and, after 14 days from the onset of the experiment, the Δ value was 0.30 ± 0.03 (Fig. 3; Table 1). Isolated particles
63 were observed in the highly viscous sol under an optical microscope (Figs. 4A and S1A) and they were identified as calcite by X-
64 ray diffraction (Fig. S2). Calcite appeared as crystals from 75 to 200 μm long, displaying rhombohedral $\{10.4\}$ faces plus less
65 developed $\{hk.0\}$ faces (Fig. 5A), as already reported.^{28, 29}



66 Figure 3. Graphical representation of the measured parameters in the precipitation experiments of calcium carbonate carried out by CDS. In the absence (A) and in
67 the presence of SOMs from *B. europaea*, at concentration *c* (B) and *5c* (C), and from *L. pruvoti*, at concentration *c* (D) and *5c* (E). The left-column refers to the highly
68 viscous sol experiments, medium-column to the gel experiments and right-column to the highly viscous sol experiments adding Mg^{2+} in the cation reservoir. The
69 length of the tubs has been normalized from cation reservoir (0) to anion reservoir (1). The real length of the U-tubs was 45 mm. Red and blue colours indicate the
70 crystallization region from the starting point of crystallization (x_o , bold numbers) to the cation reservoir (left-lower corner) and anion reservoir (right-lower corner),
71 respectively. Arrows indicate the waiting time (t_w , hours, left-upper corner) and the number of replica is shown in the right-upper corner. Horizontal black lines in the
72 middle of each figure and vertical grey lines on the arrow show the variability in the measurements. Phases were also indicated as calcite (C), Mg-calcite (MgC) and A
73 (aragonite).
74

75 **Calcium carbonate precipitation in the highly viscous sol containing SOMs by CDS.** The *Beu*SOM was added to the highly
76 viscous sol at concentrations of 50 $\mu\text{g/mL}$ (*c*) or 250 $\mu\text{g/mL}$ (*5c*). Under these conditions, t_w was 32 ± 8 hr and 52 ± 4 hr and x_o was
77 of 0.66 ± 0.04 and 0.69 ± 0.05 , respectively. The precipitation evolved asymmetrically with respect to x_o and roughly stopped in
78 the position 0.60 ± 0.01 and 0.64 ± 0.02 in the cationic reservoir direction and in the position 0.70 ± 0.03 and 0.73 ± 0.02 in the
79 anionic reservoir direction, using *Beu*SOM concentrations equal to *c* and *5c*, respectively (Fig. 3; Table 1). The optical microscope
80 pictures showed crystalline agglomerates of 100 to 400 μm , when *Beu*SOM *c* was used (Fig. 4D). Increasing the concentration of
81 *Beu*SOM up to *5c* a continuum of particles whose sizes vary between 10 and 90 μm was observed (Fig. 4G). SEM images showed
82 that these crystalline particles consisted of interconnected and prismatic-shaped nanoparticles, which formed a microscopically
83 layered structure (Fig. 6B and D). When *Beu*SOM *5c* was used a little distortion of the layered structure and a rounding at the
84 edges of the particles was observed, when compared to those obtained using *Beu*SOM *c*.

85 The dissolution of *Lpr*SOM at concentrations of 50 $\mu\text{g/mL}$ (*c*) and 250 $\mu\text{g/mL}$ (*5c*) into the highly viscous sol resulted in t_w values
86 of 37 ± 15 hr and of 41 ± 16 hr and x_o of 0.65 ± 0.05 and 0.68 ± 0.03 for concentrations *c* and *5c*, respectively. In both cases the
87 precipitation evolved symmetrically with respect to x_o . Under the optical microscope (Fig. 4J and M) the precipitates appeared to
88 be formed by agglomerated particles. The increase of concentration of *Lpr*SOM from *c* to *5c* caused a decrease in the size of the
89 particles from 60-250 μm to 15-80 μm , respectively, and sharper borders of the crystallization space (Δ). The SEM images showed
90 that the precipitates consisted of spherulitic particles (Fig 7A and C; Fig. S4) with a textural organization similar to that observed
91 in the presence of *Beu*SOM *c* (Fig. 7B). Calcite was the only phase detected by X-ray powder diffraction (Fig. S2).

92
93
94
95

Table 1. Summary of data from precipitation experiments of calcium carbonate by CDS in the absence and in the presence of SOM from *B. europaea* or *L. pruvoti*, entrapped in highly agarose viscous sol or gel and in the presence of Mg^{2+} in the cationic reservoir. The precipitation parameters refer to measures of the mineral precipitated in the U-tube: starting point of precipitation (x_0); length of the region around x_0 (Δ); waiting time (t_w). The precipitate features refer to the minerals after removal from the agarose media.

	Viscous Sol					Gel					Viscous Sol ($Mg^{2+}/Ca^{2+}=3$)				
	ref.	<i>Beu</i> <i>c</i>	<i>Beu</i> <i>5c</i>	<i>Lpr</i> <i>c</i>	<i>Lpr</i> <i>5c</i>	ref.	<i>Beu</i> <i>c</i>	<i>Beu</i> <i>5c</i>	<i>Lpr</i> <i>c</i>	<i>Lpr</i> <i>5c</i>	ref.	<i>Beu</i> <i>c</i>	<i>Beu</i> <i>5c</i>	<i>Lpr</i> <i>c</i>	<i>Lpr</i> <i>5c</i>
x_0 *	0.62 (0.05)	0.66 (0.04)	0.69 (0.05)	0.65 (0.05)	0.68 (0.03)	0.64 (0.01)	0.62 (0.00)	0.66 (0.07)	0.71 (0.01)	0.70 (0.09)	0.63 (0.03)	0.72 (0.06)	0.74 (0.08)	0.65 (0.08)	0.73 (0.09)
t_w **	22 (8)	32 (8)	52 (4)	37 (15)	41 (16)	31 (10)	37 (9)	51 (10)	53 (3)	51 (10)	34 (11)	50 (15)	74 (31)	64 (57)	73 (51)
Δ	0.30 (0.03)	0.09 (0.03)	0.10 (0.03)	0.08 (0.02)	0.08 (0.02)	0.33 (0.00)	0.11 (0.03)	0.10 (0.02)	0.08 (0.01)	0.06 (0.01)	0.35 (0.04)	0.13 (0.02)	0.03 (0.01)	0.05 (0.02)	0.04 (0.01)
phase [†]	C	C	C	C	C	C	C	C	C	C	MgC A	A MgC	MgC A	A MgC	MgC A
shape	<i>rhom.</i>	<i>r. ag.</i>	<i>sp. ag.</i>	<i>r. ag.</i>	<i>s. ag.</i>	<i>rhom</i>	<i>r. ag.</i>	<i>s. ag.</i>	<i>r. ag.</i>	<i>sp. ag.</i>	<i>ac. sp.</i>	<i>sm. sp.</i>	<i>sm. s.</i> <i>sp. ag.</i>	<i>sm. sp.</i> <i>sp. ag.</i>	<i>sm sp</i> <i>sp. ag.</i>
size ^{&}	75- 200	100- 400	10-90 300	60- 250	15- 80	80- 150	100- 500	80- 400	100- 300	15- 50	80- 150	80- 150	30- 350	100- 300	20- 300

96 * These values are normalized with respect to the length of the U-tube from the cation (0) to the anion reservoir (1). Their associated standard deviations are
97 reported in parentheses. ** The value of t_w is measured in hours. Precipitated mineral phase: C, MgC and A indicate calcite, Mg-calcite and aragonite,
98 respectively. Shape of crystals observed by SEM: *rhom.* indicates modified rhombohedra; *r. ag.* indicates agglomerates of modified rhombohedra; *sp.* indicates
99 spherulites; *ac. sp.* indicates acicular spherulites; *sm. sp.* indicates spherulites with smooth surface; *sp. ag.* indicates agglomerates of spherulites. & indicates
100 size distribution of precipitates measured along the main axis (μm). All standard deviations are reported within parenthesis.

101 **Calcium carbonate precipitation in the gel containing SOMs by CDS.** These experiments were carried out to study the
102 influence of the increased degree of entanglement of agarose molecules in the calcium carbonate precipitation process. Increasing
103 agarose concentration from 0.1% (w/v) to 0.2% (w/v) resulted in longer t_w values (Table 1). When SOMs *5c* were used, the
104 position of x_0 appeared closer to the anionic reservoir than in the pure gel reference experiment (Fig. 3). When *Beu*SOM *c*
105 was added x_0 did not differ from the reference experiment, while a significant shift towards the anionic reservoir was observed using
106 *Lpr*SOM *c*. The values of Δ and its evolution with the time did not vary using the gel instead of the highly viscous sol. Only when
107 using *Lpr*SOM *c*, the precipitation evolved asymmetrically with respect to x_0 (0.71 ± 0.01), being Δ longer toward the cationic
108 reservoir (0.64 ± 0.02) than toward the anionic one (0.72 ± 0.01).
109
110

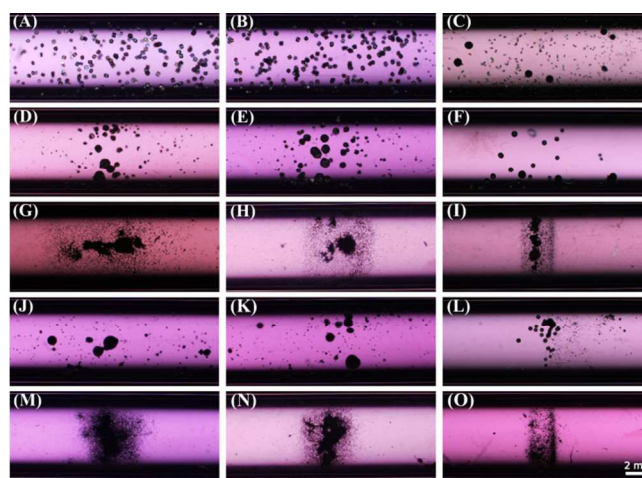
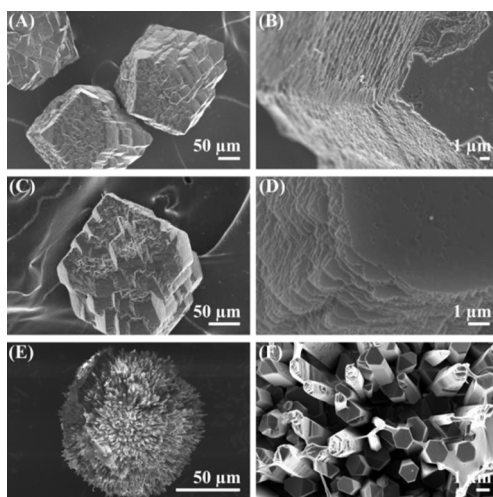
111
112
113
114

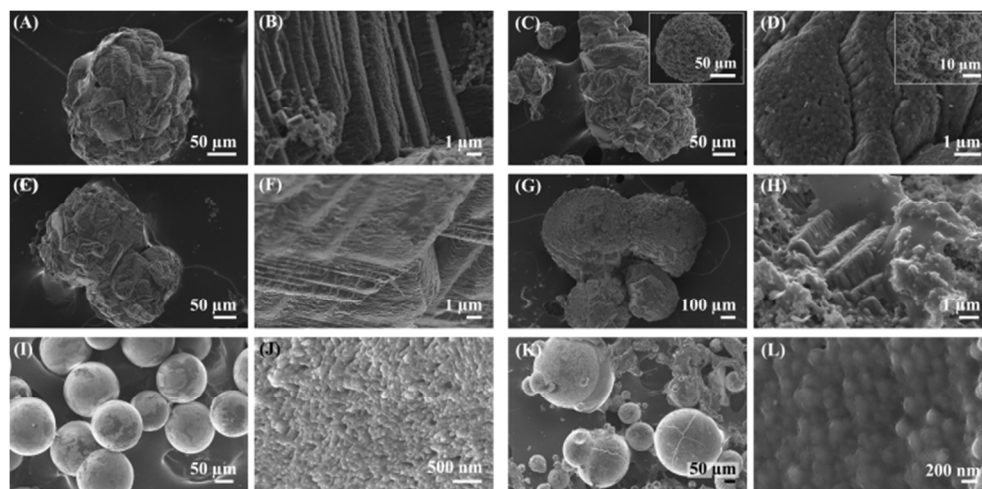
Figure 4. Optical microscope images of crystal growing spaces (Δ) after 14 days, in the absence (A-C) and in the presence of SOMs from *B. europaea*, at concentration *c* (D-F) and *5c* (G-I), and from *L. pruvoti*, at concentration *c* (J-L) and *5c* (M-O). The left-column refers to the highly viscous sol experiments, the medium-column to the gel experiments and the right-column to the highly viscous sol experiments, adding Mg^{2+} into the cationic reservoir.

115 Optical microscope pictures of Δ showed that in the gel the differences observed among trials were enhanced with respect to the
 116 highly viscous sol (Fig. 4), especially in the presence of *LprSOM*. Particularly, sharper Δ borders were observed using SOMs *5c*.
 117 The particles showed morphologies and size distributions similar to those observed in the highly viscous sol (Figs. 5, 6 and 7).
 118 Only when *LprSOM 5c* was used smaller crystals (15-50 μm) were observed (Fig. S4). Calcite was the only phase detected by X-
 119 ray powder diffraction.



120 Figure 5. SEM pictures showing the morphology of calcium carbonate crystals formed in highly agarose viscous sol in the absence of SOMs. The first row shows the
 121 CaCO_3 crystals grown in highly agarose viscous sol (A, B); the second row, in agarose gel (C, D); and the third row, in highly agarose viscous sol with the addition of
 122 Mg^{2+} into the cation reservoir (E, F). The columns show different magnifications. The morphology of precipitates did not allow to distinguish between the two phases
 123 detected by XRD and FTIR analysis in the experiments carried out with added Mg^{2+} . These images are representative of the whole sample populations.
 124

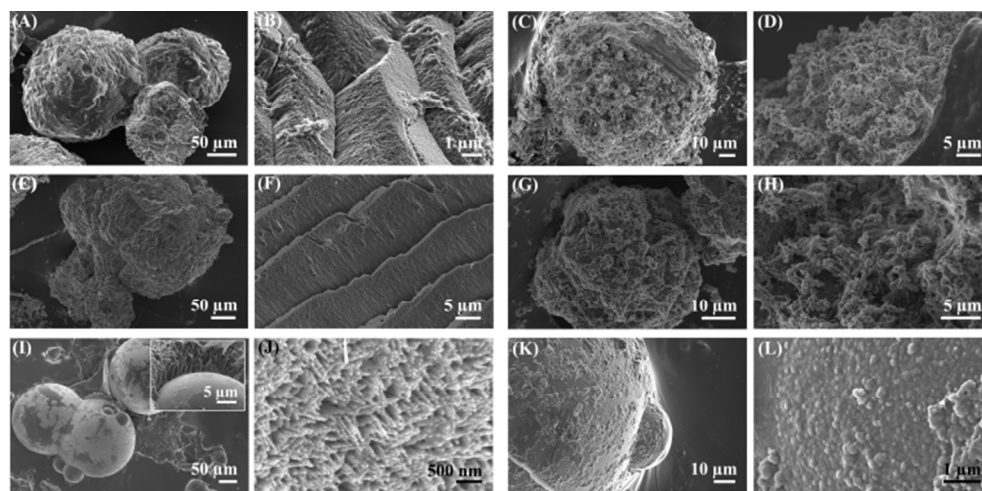
125 **Calcium carbonate precipitation in highly viscous sol containing SOMs and diffusing Mg^{2+} by CDS.** The addition of Mg^{2+} in
 126 the cationic reservoir (Mg/Ca molar ratio equal to 3) always led to an increase of t_w and a shift of x_o toward the anionic reservoir.
 127 Interestingly, in the presence of *LprSOM c* the x_o value (0.65 ± 0.08) was similar to that obtained in the absence of Mg^{2+} . In the
 128 presence of diffusing Mg^{2+} the length of Δ from x_o to the cationic reservoir was greater than toward the anionic one (0.24 ± 0.06
 129 and 0.11 ± 0.03 , respectively). The Δ values were shorter than those observed in the Mg^{2+} free experiments (Fig. 3; Table 1).



130 Figure 6. SEM pictures showing the morphology of crystals formed in the presence of SOMs from *B. europaea*. The micrographs A, B, E, F, I and J show crystals
 131 obtained in the presence of *BeuSOM c* whereas images C, D, G, H, K and L show crystals obtained in the presence of *BeuSOM 5c*. The first row (pictures A-D)
 132 corresponds to the highly agarose viscous sol experiments; the second row (E-H), with the agarose gel experiments and the third row (I-L), with the agarose highly
 133 viscous sol experiments with diffusing Mg^{2+} . The micrograph C and the inset show the two different morphologies of the precipitates formed in this condition. The
 134 inset of D is a high magnification of the spherulite showed in the inset of C. The observed morphologies of the precipitates obtained in the presence of Mg^{2+} (third
 135 row) did not allow to distinguish between MgC and A , which were detected by XRD and FTIR analysis. These images are representative of the whole sample
 136 populations (Fig. S4).
 137

138 In highly viscous sol Mg^{2+} favoured the precipitation of large rounded and small peanuts-shaped particles (Fig. 4C). The addition
 139 of SOMs brought about a reduction of crystallization density. Spherical and isolated particles were always observed when SOM *c*

140 was used, while when using SOMs 5c, the particles were more aggregated and sharp Δ borders were observed, closer to the
 141 anionic reservoir (Fig. 4). In the latter condition, agglomerates in addition to small particles were obtained. The spherulites
 142 observed in the reference experiment were composed of hexagonal needle-shaped microcrystallites (Fig. 5F). Slight morphological
 143 changes were observed by adding *Beu*SOM or *Lpr*SOM, while the concentration effect of SOM was more relevant. Using SOM *c*
 144 the size of crystals was more homogeneous than that obtained using SOM 5c (Fig. S4). This observation agrees with the crystal
 145 aggregation observed in optical microscope pictures (Figs. 4 and S1). The presence of SOMs and diffusing Mg^{2+} made the
 146 prismatic crystals thinner, sharper and more co-oriented with respect to those obtained in the reference experiments. Using SOM
 147 5c spherulites displaying rough surfaces (Fig. 6L and Fig. 7L) were observed instead of the needle-shaped agglomerates.
 148 Aragonites and Mg-calcite were identified by X-ray diffraction and FTIR spectroscopy in all cases (Figs. S2 and S3). The
 149 quantitative Mg-calcite/aragonite mass ratio (Fig. 8) was measured analyzing the FTIR spectra. This ratio either increased or
 150 decreased with respect to the reference when SOM *c* or SOM 5c were used, respectively.

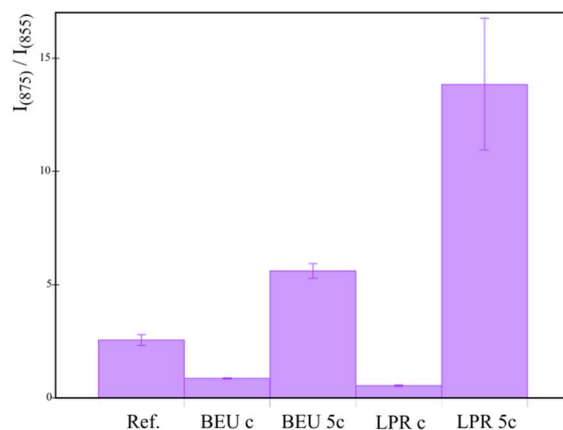


151
 152
 153
 154
 155
 156
 157
 Figure 7. SEM pictures showing the morphology of crystals formed in the presence of SOM from *L. pruvoti*. The micrographs A, B, E, F, I and J show crystals obtained in the presence of *Lpr*SOM *c* whereas images C, D, G, H, K and L show crystals obtained in the presence of *Lpr*SOM 5c. The first row (pictures A-D) corresponds to the highly agarose viscous sol experiments; the second row (E-H), with the agarose gel experiments and the third row (I-L), with the highly agarose viscous sol experiments with diffusing Mg^{2+} . The inset in picture I shows a higher magnification of the peanut-like crystals. The observed morphologies of the precipitates obtained in the presence of Mg^{2+} (third row) did not allow to distinguish between MgC and A, which were the phases detected by XRD and FTIR analysis. These images are representative of the whole sample populations (Fig. S4).

158 Discussion

159 Coral biomineralization occurs in a gel-like environment.⁴ CDS has proven to be a valid tool to study the role of additives in
 160 nucleation/growth processes of calcium carbonate in such medium.^{30, 31} Thus, the use of the CDS in the presence of SOMs from
 161 the solitary Mediterranean coral *B. europaea* or *L. pruvoti* allows to investigate differences and similarities in calcification
 162 between zooxanthellated and azooxanthellated species. To achieve this goal, a series of *in vitro* crystallization trials, with two
 163 concentrations of SOMs, different viscosity of the media and in the presence of diffusing Mg^{2+} , were carried out. In the reference
 164 experiments (i.e. the ones without SOMs entrapped in the highly viscous sol or gel) the first precipitates appeared in the same sites
 165 (x_0), situated in the vicinity of the anionic reservoir (Table 1). The x_0 value must fulfil the equivalence rule^{17, 22, 30, 31} and at this
 166 point, the ion activity product has to overcome the critical value needed to induce nucleation. x_0 is displaced to the right of the U-
 167 tube (closer to HCO_3^-/CO_3^{2-} reservoir) due to the much lower initial CO_3^{2-} concentration of this solution compared to that of Ca^{2+}
 168 ions.³⁰ The data also show that x_0 is not affected by the degree of entanglement of the agarose molecules (i.e. no difference was
 169 observed between the highly viscous sol and the gel). This indicates that the diffusion rate of Ca^{2+} and carbonate species was
 170 equally affected by the different porosity of the two media. Interestingly, x_0 values did not change in the experiments in the
 171 presence of Mg^{2+} (the concentration of Ca^{2+} was reduced to keep constant the ionic strength of the cationic reservoir solution).
 172 This apparent violation of the equivalence rule could be justified considering that Mg^{2+} can interact with CO_3^{2-} as Ca^{2+} does;
 173 although with less strength (the solubility of calcium carbonate is lower than that of magnesium carbonate). Thus, the activity of
 174 CO_3^{2-} interacting with Ca^{2+} is reduced proportionally to the Mg/Ca molar ratio and the precipitation occurred in conditions as if the
 175 activity of CO_3^{2-} was lower. This hypothesis implies a longer t_w , as it was indeed observed. A contribution to the increase of t_w
 176 comes also from the inhibition of calcite growth due to the adsorption of Mg^{2+} on the calcite nuclei.^{32, 33} Diffusion of Mg^{2+} did not
 177 change significantly the Δ -values, but affected the symmetry of the growing front. The boundaries of the crystal growing spaces
 178 (Δ) represent the places where the activity of anions -in the zone close to the cationic reservoir- and the activity of cations -in the
 179 zone close to the anionic one- are the lowest to still sustain nucleation and growth of crystals. Here, it is showed that Mg^{2+} inhibits

180 only the growth process, as indicated by the similar Δ -values.³⁰ Besides, Δ cannot be symmetric around x_0 , in this case the growing
 181 space starting from x_0 up to the last observed crystals in the direction to the cationic reservoir was longer to that in the direction to
 182 the anionic one. This asymmetry suggests a different range of ionic activity of cations and anions to sustain nucleation and growth,
 183 and also could be a result of the lower activity of Ca^{2+} compare to that in the reference.
 184 The addition of *BeuSOM* or *LprSOM* to the highly viscous sol, or the gel, increased the t_w and slightly shifted the x_0 positions in
 185 the direction of the anionic reservoir. These effects were more marked when using the higher concentration of SOMs. The longer
 186 t_w with respect to the reference experiment most likely indicated an inhibition of the nucleation and/or incipient growth processes.
 187 Since in the presence of SOMs the Δ -values were shortened, an inhibition of the nucleation event was evident. Moreover, the
 188 morphology of the crystals was influenced by the presence of SOMs, suggesting that an inhibition of the growth process was
 189 present as well. The shift of x_0 , which showed a trend, suggested that the presence of SOMs influenced the speciation of carbonate.
 190 Since *LprSOM* and *BeuSOM* contain acidic macromolecules characterized in their proteic regions by the presence of high
 191 percentage (almost 50 mol %) of aspartic and glutamic residues and glycosylated regions rich in sulphate groups, it can be
 192 supposed that their carboxylic group ($\text{p}K_a$ around 4.5) could release protons in the highly viscous sol or in the gel, slightly
 193 reducing the activity of the carbonate ions in favour of that of hydrogen carbonate, but this was not observed in the presence of
 194 charged polypeptides.³⁰ On the other hand, it is also known that SOM is composed of intrinsically disordered proteins, IDPs.^{34, 35}
 195 The IDPs could locally change their ability to interact with diffusing ions due to their high structural flexibility. It is also note
 196 worth that SOMs also contain glycoproteins in which the $\text{p}K_a$ changes, and therefore the ability to chelate calcium ions, with the
 197 degree of grafting.³⁶ Finally, the presence of lipids could have also an important role in stabilizing transient amorphous calcium
 198 carbonate forms.¹⁵ Since SOMs are macromolecular mixtures, to specify a role for each organic component a further detailed study
 199 would be required.



200 Figure 8. Area ratios of the 875 cm^{-1} and the 855 cm^{-1} deconvoluted bands of precipitates. This area ratio represents a rough estimation of the Mg-calcite/aragonite
 201 mass ratio. The error bars were calculated by using the first-order Taylor method for propagating uncertainties considering the standard deviations associated with
 202 each area value.
 203

204 We found that when increasing the degree of entanglement and the concentration of SOMs the Δ borders became closer and
 205 sharper. In these conditions a lower ionic diffusion rate, a more confined space for the nucleation and growth of crystals and a
 206 higher SOMs inhibition effect, were present. The fact that the presence of Mg^{2+} made these borders even sharper suggested that
 207 Mg^{2+} could have a role in confining the crystallization conditions within defined calcium carbonate supersaturation values, as
 208 observed in the presence of *BeuSOM* or *LprSOM*.
 209 In the presence of Mg^{2+} , the SOMs provoked a shift of x_0 towards the anionic reservoir (as observed in the absence of Mg^{2+}), a
 210 longer t_w and co-precipitation of aragonite with Mg-calcite. Interestingly the Mg-calcite / aragonite mass ratio was altered as a
 211 function of the concentration of SOMs; the low concentration (*c*) favoured the precipitation of aragonite while the high
 212 concentration (*5c*) favoured that of Mg-calcite (Fig. 8). This effect was more pronounced when using *LprSOM*. This Janus
 213 behaviour -the capability of the same family of molecules to promote and inhibit one phase- has been recently demonstrated for
 214 several additives in solution and in solid state.³⁷ Here, this behaviour can be justified in the context of the basic principles of
 215 biomineralization. Certain SOMs molecules are able to interact with aragonite crystals, probably on specific crystalline planes.
 216 These molecules, when present in low concentration can act as nucleation sites for aragonite and / or inhibition of calcite by Mg^{2+} ,
 217 thus favouring aragonite precipitation. When the concentration is high they are able to interact with the growing nuclei and / or
 218 enhanced magnesium dehydration,³⁸ and thus giving as net result the inhibition of the precipitation of aragonite.

219 An intriguing effect of the interaction between Mg^{2+} and SOM was the nanoscale size of the crystals. The SEM images (Fig. 6L
220 and Fig. 7L) show a granular structure when crystals grew in a highly viscous sol entrapping SOM and Mg^{2+} were diffusing along
221 the tube. This structure is very similar to that observed for corals by Falini *et al.*¹⁶ in *in vitro* calcification experiments, by
222 Vandermeulen and Watabe³⁹ and Motai *et al.*⁴⁰ in *in vivo* studies as well as in biominerals from different phyla.^{41, 42} This
223 granulated texture was identified as formed from amorphous calcium carbonate domains in sea urchin spicule⁴³ and cystoliths.⁴⁴
224 Pai and Pillai^{45, 46} proposed the formation of hollow triangular calcium carbonate forms from amorphous calcium carbonate
225 spherical aggregates stabilized by the change in the conformation of a synthetic polypeptide induced by the presence of Mg^{2+} .
226 These observations suggested a synergic role between SOMs and Mg^{2+} , which starts with a common amorphous precursor that
227 later on transforms to aragonite or Mg-calcite depending on SOM concentration.
228 The stronger effect on crystallization parameters observed by the addition of *Lpr*SOM with respect to *Beu*SOM along to the higher
229 impact on the crystal morphology cannot be only justified on the basis of the different amino acidic composition. Indeed, in
230 several models of biomineralization a more efficient role of acidic macromolecules, as calcium carbonate crystallization modifiers,
231 has been related to a higher content of ionisable functional groups.^{25, 26, 36, 38, 47, 48} The used SOMs also differ in their glycosidic
232 region structures and in the content of lipids. *Lpr*SOM has a higher degree of sulphonation along its glycosidic chains (Fig. 2, band
233 at 1147 cm^{-1}) and presents a higher content of lipids. These two features entail an additional content of acidic functional groups
234 compared to that due only to proteins. Sulphate groups in corals are mainly localized in the skeletal textural region referred as
235 *center of calcification*,⁴¹ which represents the zone where the skeleton coral growth starts. Thus, in addition to the above proposed
236 effects, the favoured precipitation of Mg-calcite in the presence of *Lpr*SOM could be also due to the different structure of the
237 polysaccharide chains as well as to a reduced activity of Mg^{2+} in their presence.⁴⁹⁻⁵²
238 The diverse distribution of molecules in the two SOMs, and their different impact on the precipitation of calcium carbonate could
239 be related to the presence/absence of zooxanthella. It has been already shown that zooxanthellate and azooxanthellate corals differ
240 in their average amino acidic composition, being the latter richer in acidic residues.⁵³ Here, it was observed that differences are
241 also in the content of lipids and in the structure and functionalization of polysaccharides. Zooxanthella provide an energetic
242 support to calcification through photosynthesis⁵⁴ and it has been reported that they may influence the speciation of the inorganic
243 carbon affecting the trafficking of protons around the nucleation site. Thus, it could be speculated that various molecular actors
244 play a different role in the presence of photosynthesis in coral biomineralization.
245

246 Experimental

247 **Coral skeletons.** Samples of *Balanophyllia europaea* and *Leptopsammia pruvoti* were randomly collected during scuba diving in
248 the North-Western Mediterranean Sea, at Calafuria 43°27'N, 10°21'E. *B. europaea* was collected at 6 m depth; *L. pruvoti* at 16 m
249 depth. After collection the corals were dipped in a sodium hypochlorite solution (commercial) for 4 days until the polyp tissue was
250 completely dissolved, then the remaining skeletons were washed with double distilled water and dried in an oven at 37 °C for 24
251 hr. and stored. Each skeleton was analysed under a binocular microscope to remove fragment of substratum and calcareous
252 deposits produced by other organisms. Successively, the skeletons were ground in a mortar to obtain a fine and homogeneous
253 powder. The obtained powder was subsequently suspended (1% w/v) in a sodium hypochlorite solution (3% v/v) to remove traces
254 of organic material not removed by the first treatment.

255 **Extraction of the soluble organic matrix (SOM).** Five mL of milli-Q water, in which 2.5 g of powdered coral skeleton were
256 dispersed, were poured into a 40 cm-long osmotic tube for dialysis (MWCO = 3.5 kDa; CelluSep®, MFPI). The sealed tube was
257 placed into 1 L of 0.1M CH_3COOH (Riedel de Haen) solution under stirring. The decalcification proceeded for 72 hr. At the end
258 the tube containing the dissolved OM was dialysed against milli-Q water (resistivity 18.2 M Ω cm at 25 °C; filtered through a 0.22
259 μm membrane) until the final pH was about 6. The obtained aqueous solution containing the OM was centrifuged at 30 g for 5
260 minutes to separate the soluble (SOM) and the insoluble (IOM) OM fractions, which were then lyophilized and weighed.

261 **Preparation of agarose highly viscous sol and gel.** Firstly, an agarose stock solution of 0.3% (w/v) was heated up to 90 °C for 20
262 minutes to dissolve completely the agarose powder (Agarose D-5, Hispanagar). Then, the solution was cooled down (to about 40
263 °C) and thereafter mixed with the required volume of heated milli-Q water in different beakers partially submerged in a water bath
264 at 50 °C to obtain final 0.1% or 0.2% (w/v) agarose solutions. In each beaker a different amount of dissolved *Beu*SOM or *Lpr*SOM
265 was added to reach a final concentration of 50 $\mu g/mL$ (*c*) or 250 $\mu g/mL$ (*5c*). The prepared solution was vortex during 1 min and
266 transferred to U-tubes with a 1 mL syringe.

267 **Calcium carbonate precipitation by CDS.** The experiments were carried out by using a U-tube system (Triana Science &
268 Technology, S.L, Granada, Spain). These tubes have a column length of 45 mm, which is accessible to diffusing reagents from two
269 side source reservoirs. To the cation reservoir 0.2 mL of a 0.5 M solution with Mg/Ca ratio equal to 0 or 3 were added. These
270 solutions were prepared by mixing $CaCl_2 \cdot 2H_2O$ and $MgCl_2 \cdot 6H_2O$ (Sigma-Aldrich). To the anion reservoir 0.2 mL of 0.5 M
271 $NaHCO_3$ solution (Fluka Biochemika) were added. The initial pHs of the solutions were: 5.7 for 0.5 M $CaCl_2$; 6.2 for 0.5 M
272 $CaCl_2/MgCl_2$; and 8.1 for 0.5 M $NaHCO_3$. Cation and anion solutions counter-diffused through the column filled with an agarose

273 highly viscous sol entrapping the SOMs. In the U-tube set up we measured three main parameters: the waiting time (t_w) or time
274 that elapsed from the onset of the experiment up to the appearance of the first precipitate (observed under an optical microscope at
275 magnification 4x); the starting point of precipitation (x_0) or the distance from the cationic reservoir to the place where the first
276 crystals appeared and the crystal growing space (Δ) or the length within the column gel where precipitates were observed after 14
277 days from the onset of the experiment.³⁰ The pH values of the reservoirs did not change after the precipitation experiments.
278 Precipitates were taken out from the tube and placed on top of a 0.45 μm pore size filter. The precipitates were washed several
279 times with hot milli-Q water in order to remove agarose and then air-dried. All the experiments were performed at room
280 temperature.

281 **Characterization of CaCO_3 precipitates.** Optical microscope (OM) observations were made using a Nikon AZ100 optical
282 microscope connected to a digital camera (Nikon, DS-Fi1). Some samples were inspected by a PhenomTM scanning electron
283 microscope (SEM). In addition, scanning electron micrographs of carbon-sputtered samples were collected using a GEMINI Carl
284 Zeiss SMT field emission scanning electron microscope. The structural properties of the precipitates were analysed by X-ray
285 diffraction (XRD) and Fourier transform infrared spectroscopy (FTIR). Therefore, the crystals were ground and mounted on a
286 Bruker X8 Proteum diffractometer equipped with a Microstar copper rotating anode generator, a κ goniometer, and a SMART
287 6000 CCD detector. The calculated XRD powder diffraction patterns were obtained after integrating the diffraction frames with
288 the XRD2DSCAN.⁵⁵ Fourier transform infrared (FTIR) spectroscopy analyses were collected using a FTIR Nicolet 380 instrument
289 (Thermo Electron Co.) from 4000 to 400 cm^{-1} at a resolution of 4 cm^{-1} . Disks were made by applying a pressure of 48.6 psi to a
290 mixture consisting of 1 mg of sample and 100 mg of KBr by means of a hydraulic press. Mg-calcite to aragonite mass ratios
291 semiquantitative analysis was performed integrating the deconvoluted bands at 875 cm^{-1} for calcite and at 855 cm^{-1} for aragonite.
292 The error bars were calculated by using the first-order Taylor method for propagating uncertainties considering the standard
293 deviation associated with each area value.⁵⁶
294

295 Conclusions

296 Here, a study on CaCO_3 precipitation in agarose highly viscous sol and agarose gel hosting SOMs from two corals and diffusing
297 Mg^{2+} , is presented. The main results are the following: (i) the molecular composition of the two SOMs has a different impact on
298 the crystallization parameters and morphology of CaCO_3 ; (ii) the viscosity of the gelling media, and thus its porosity, is important
299 in regulating the SOM action; (iii) Mg^{2+} have a notable role in defining specific, and sharp, limits of supersaturation under which
300 precipitation occurs as well as in phase selection; (iv) the phase distribution is affected by the SOM concentration. Thus, through
301 the use of the CDS, it was possible to carry out a first study on *in vitro* biomineralization of a zooxanthellate and an
302 azooxanthellate coral.
303
304

305 Acknowledgements

306 The research leading to these results has received funding from the European Research Council under the European Union's
307 Seventh Framework Programme (FP7/2007-2013)/ERC grant agreement n° [249930–CoralWarm: Corals and global warming: the
308 Mediterranean versus the Red Sea] and from Excellence project RNM5384 of Junta de Andalucía. M.S.T. also thanks to CSIC for
309 her JAE-Pre research contract within the “Junta para la Ampliación de Estudios” co-funded by the European Social Found (ESF).
310 We deeply thank Gianni Neto for the coral underwater pictures. GF and SF thank the Consorzio Interuniversitario di Ricerca della
311 Chimica dei Metalli nei Sistemi Biologici (CIRC MSB) for the support.
312
313

314 Notes and references

315 ^a Laboratorio de Estudios Cristalográficos, IACT (CSIC-UGR). Avda. Las Palmeras, n° 4. E-18100 Armilla, Spain.

316 ^b Dipartimento di Chimica “G. Ciamician”, Alma Mater Studiorum Università di Bologna, via Selmi 2, I-40126 Bologna, Italy.

317 ^c Marine Science Group, Department of Biological, Geological and Environmental Sciences, Section of Biology, Alma Mater Studiorum University of
318 Bologna, Via Selmi 3, 40126 Bologna, Italy.

319 ^d The Mina and Everard Goodman Faculty of Life Sciences, Bar Ilan University, Ramat Gan, Israel.

320 *Corresponding authors: Giuseppe Falini (giuseppe.falini@unibo.it), Jaime Gómez-Morales (jaime@lec.csic.es)
321

322 † Electronic Supplementary Information (ESI) available: Optical microscope images, XRD patterns, FTIR spectra and low-magnification SEM
323 pictures of calcium carbonate precipitates. See DOI: 10.1039/b000000x/
324
325
326

327 **Abbreviations**

328 CaCO₃, calcium carbonate; Mg²⁺, Ca²⁺ and CO₃²⁻, magnesium, calcium and carbonate ions; CDS, counter-diffusion system; SOM, soluble organic
329 matrix; *Beu*SOM and *Lpr*SOM, soluble organic matrix from *Balanophyllia europaea* and *Leptosammia pruvoti*; *c* and *5c*, soluble organic matrix
330 concentrations of 50 µg/mL and 250 µg/mL; *t*_{vis}, waiting time; *x*₀, starting point of precipitation; and Δ, crystal growing space.

- 331
332
333 1. M. D. Spalding, C. Ravilious and E. P. Green, "World atlas of coral reefs". Univ of California Press, Berkeley, 2001.
334 2. A. L. Cohen and T. A. McConnaughey, *Rev. Mineral. Geochem.*, 2003, **54**, 151-187.
335 3. A. T. Marshall and P. Clode, *Coral Reefs*, 2004, **23**, 218-224.
336 4. S. Tambutté, M. Holcomb, C. Ferrier-Pagès, S. Reynaud, É. Tambutté, D. Zoccola and D. Allemand, *J. Exp. Mar. Biol. Ecol.*, 2011, **408**, 58-78
337 (and references therein).
338 5. M. Wilfert and W. Peters, *Z. Morph. Tiere*, 1969, **64**, 77-84.
339 6. S. D. Young, *Comp. Biochem. Physiol., Part B: Comp. Biochem.*, 1971, **40**, 113-120.
340 7. D. J. Barnes, *Science*, 1970, **170**, 1305-1308.
341 8. J. P. Cuif, Y. Dauphin, J. Doucet, M. Salome and J. Susini, *Geochim. Cosmochim. Acta*, 2003, **67**, 75-83.
342 9. J. P. Cuif and Y. Dauphin, *J. Struct. Biol.*, 2005, **150**, 319-331.
343 10. I. S. Johnston, *Int. Rev. Cytol.*, 1980, **67**, 171-214.
344 11. W. H. Bryan and D. Hill, *Proc. R. Soc. Queensl.*, 1941, **52**, 78-91.
345 12. A. C. Gagnon, J. F. Adkins and J. Erez, *Earth Planet. Sci. Lett.*, 2012, **329-330**, 150-161.
346 13. A. A. Venn, E. Tambutté, M. Holcomb, J. Laurent, D. Allemand and S. Tambutté, *Proc. Natl. Acad. Sci.*, 2013, **110**, 1634-1639.
347 14. L. Fernandez-Diaz, A. Putnis, M. Prieto and C. V. Putnis, *J. Sediment. Res.*, 1996, **66**, 482-491.
348 15. S. Goffredo, P. Vergni, M. Reggi, E. Caroselli, F. Sparla, O. Levy, Z. Dubinsky and G. Falini, *PLoS One*, 2011, **6**, e22338.
349 16. G. Falini, M. Reggi, S. Fermani, F. Sparla, S. Goffredo, Z. Dubinsky, O. Levi, Y. Dauphin and J. P. Cuif, *J. Struct. Biol.*, 2013, **183**, 226-238.
350 17. T. Mass, J. L. Drake, L. Haramaty, J. D. Kim, E. Zelzion, D. Bhattacharya and P. G. Falkowski, *Curr. Biol.*, 2013, **23**, 1126-1131.
351 18. H. K. Henisch and J. M. García-Ruiz, *J. Cryst. Growth*, 1986, **75**, 195-202.
352 19. M. Prieto, A. Putnis, L. Fernández-Díaz and S. López-Andrés, *J. Cryst. Growth*, 1994, **142**, 225-235.
353 20. A. Dey, G. de With and N. A. J. M. Sommerdijk, *Chem. Soc. Rev.*, 2010, **39**, 397-409.
354 21. D. Allemand, C. Ferrier-Pagès, P. Furla, F. Houlbrèque, S. Puverel, S. Reynaud, É. Tambutté, S. Tambutté and D. Zoccola, *C. R. Acad. Sci.*, 2004,
355 **3**, 453-467.
356 22. M. F. Colombo-Pallotta, A. Rodríguez-Román and R. Iglesias-Prieto, *Coral Reefs*, 2010, **29**, 899-907.
357 23. J. M. García-Ruiz, *Key Eng. Mater.*, 1991, **58**, 87-106.
358 24. H. K. Henisch and J. M. García-Ruiz, *J. Cryst. Growth*, 1986, **75**, 203-211.
359 25. E. Asenath-Smith, H. Li, E. C. Keene, Z. W. Seh and L. A. Estroff, *Adv. Funct. Mater.*, 2012, **22**, 2891-2914.
360 26. J. R. Dorvee, A. L. Boskey and L. A. Estroff, *CrystEngComm*, 2012, **14**, 5681-5700.
361 27. F. S. Parker, "Applications of infrared, Raman, and resonance Raman spectroscopy in biochemistry". Springer, New York, 1983.
362 28. H. Li, H. L. Xin, D. A. Muller and L. A. Estroff, *Science*, 2009, **326**, 1244-1247.
363 29. H. Li and L. A. Estroff, *CrystEngComm*, 2007, **9**, 1153-1155.
364 30. M. Sancho-Tomás, S. Fermani, M. A. Durán-Olivencia, F. Otálora, J. Gómez-Morales, G. Falini and J. M. García-Ruiz, *Cryst. Growth Des.*, 2013,
365 **13**, 3884-3891.
366 31. L. A. Estroff, L. Addadi, S. Weiner and A. D. Hamilton, *Org. Biomol. Chem.*, 2004, **2**, 137-141.
367 32. F. Lippmann, "Sedimentary Carbonate Minerals: Minerals, Rocks and Inorganic Materials". Springer-Verlag Berlin, 1973.
368 33. G. Falini, S. Fermani, G. Tosi and E. Dinelli, *Cryst. Growth Des.*, 2009, **9**, 2065-2072.
369 34. A. Adamiano, S. Bonacchi, N. Calonghi, D. Fabbri, G. Falini, S. Fermani, D. Genovese, D. Kralj, M. Montalti, B. Njegić Džakula, L. Prodi and G.
370 Sartor, *Chem. Eur. J.*, 2012, **18**, 14367-14374.
371 35. M. Wojtas, P. Dobryszewski and A. Ožyhar, in *Advanced topics in biomineralization*, ed. J. Seto, InTech, 2012, ch. 1, pp. 1-32 (and references
372 therein).
373 36. D. Malferrari, S. Fermani, P. Galletti, M. Goisis, E. Tagliavini and G. Falini, *Langmuir*, 2013, **29**, 1938-1947.
374 37. J. Ihli, Y. Y. Kim, E. H. Noel and F. C. Meldrum, *Adv. Funct. Mater.*, 2013, **23**, 1575-1585.
375 38. S. Albeck, J. Aizenberg, L. Addadi and S. Weiner, *J. Am. Chem. Soc.*, 1993, **115**, 11691-11697.
376 39. J. H. Vandermeulen and N. Watabe, *Mar. Biol.*, 1973, **23**, 47-57.
377 40. S. Motai, T. Nagai, K. Sowa, T. Watanabe, N. Sakamoto, H. Yurimoto and J. Kawano, *J. Struct. Biol.*, 2012, **180**, 389-393.
378 41. J. P. Cuif, Y. Dauphin, B. Farre, G. Nehrke, J. Nouet and M. Salomé, *Mineral. Mag.*, 2008, **72**, 233-237.
379 42. J. H. E. Cartwright, A. G. Checa, J. D. Gale, D. Gebauer and C. I. Sainz-Díaz, *Angew. Chem., Int. Ed.*, 2012, **51**, 11960-11970.
380 43. Y. Politi, R. A. Metzler, M. Abrecht, B. Gilbert, F. H. Wilt, I. Sagi, L. Addadi, S. Weiner and P. U. P. A. Gilbert, *Proc. Natl. Acad. Sci.*, 2008, **105**,
381 17362-17366.

- 382 44. A. Gal, W. Habraken, D. Gur, P. Fratzl, S. Weiner and L. Addadi, *Angew. Chem.*, 2013, **125**, 4967-4970.
383 45. R. K. Pai and S. Pillai, *Cryst. Growth Des.*, 2006, **7**, 215-217.
384 46. R. K. Pai and S. Pillai, *J. Am. Chem. Soc.*, 2008, **130**, 13074-13078.
385 47. J. L. Arias and M. S. Fernández, *Chem. Rev.*, 2008, **108**, 4475-4482.
386 48. C. C. Tester, R. E. Brock, C. H. Wu, M. R. Krejci, S. Weigand and D. Joester, *CrystEngComm*, 2011, **13**, 3975-3978.
387 49. S. Weiner and L. Addadi, *Annu. Rev. Mater. Res.*, 2011, **41**, 21-40.
388 50. A. J. Giuffre, L. M. Hamm, N. Han, J. J. De Yoreo and P. M. Dove, *Proc. Natl. Acad. Sci.*, 2013, **110**, 9261-9266.
389 51. A. E. Stephenson, J. J. DeYoreo, L. Wu, K. J. Wu, J. Hoyer and P. M. Dove, *Science*, 2008, **322**, 724-727.
390 52. J. Tao, D. Zhou, Z. Zhang, X. Xu and R. Tang, *Proc. Natl. Acad. Sci.*, 2009, **106**, 22096-22101.
391 53. J. P. Cuif, Y. Dauphin, A. Freiwald, P. Gautret and H. Zibrowius, *Comp. Biochem. Physiol., Part A: Mol. Integr. Physiol.*, 1999, **123**, 269-278.
392 54. P. L. Jokiel, *Bull. Mar. Sci.*, 2011, **87**, 639-657.
393 55. A. Rodriguez-Navarro, *J. Appl. Crystallogr.*, 2006, **39**, 905-909.
394 56. S. Mekid and D. Vaja, *Measurement*, 2008, **41**, 600-609.
395
396

Table of Contents

Coral biomineralization is explored through calcium carbonate precipitation experiments, by counter-diffusion, using agarose highly viscous sol or gel entrapping soluble organic matrices extracted from *Balanophyllia europaea*, and *Leptopsammia pruvoti* species, as well as diffusing Mg^{2+} .





Graphical abstract
39x26mm (300 x 300 DPI)